Journal of Molecular Modeling (2024) 30:233
https://doi.org/10.1007/s00894-024-06032-w

ORIGINAL PAPER

Specific interaction from different $A\beta_{42}$ peptide fragments to α7nAChR-A study of molecular dynamics simulation

Xvzhi Gao[1] · Yvning Guan[1] · Chuanbo Wang[1] · Mengke Jia[1] · Sajjad Ahmad[1] · Muhammad Fahad Nouman[1] · Hongqi Ai[1]

Received: 31 March 2024 / Accepted: 18 June 2024 / Published online: 28 June 2024

Abstract

Context Existing researches confirmed that β amyloid (Aβ) has a high affinity for the α7 nicotinic acetylcholine receptor (α7nAChR), associating closely to Alzheimer's disease. The majority of related studies focused on the experimental reports on the neuroprotective role of Aβ fragment ($A\beta_x$), however, with a lack of investigation into the most suitable binding region and mechanism of action between Aβ fragment and α7nAChR. In the study, we employed four $A\beta_{1-42}$ fragments $A\beta_x$, $A\beta_{1-16}$, $A\beta_{10-16}$, $A\beta_{12-28}$, and $A\beta_{30-42}$, of which the first three were confirmed to play neuroprotective roles upon directly binding, to interact with α7nAChR.

Methods The protein–ligand docking server of CABS-DOCK was employed to obtain the α7nAChR-$A\beta_x$ complexes. Only the top α7nAChR-$A\beta_x$ complexes were used to perform all-atom GROMACS dynamics simulation in combination with Charmm36 force field, by which α7nAChR-$A\beta_x$ interactions' dynamic behavior and specific locations of these different $A\beta_x$ fragments were identified. MM-PBSA calculations were also done to estimate the binding free energies and the different contributions from the residues in the $A\beta_x$. Two distinct results for the first three and fourth $A\beta_x$ fragments in binding site, strength, key residue, and orientation, account for why the fourth fails to play a neuroprotective role at the molecular level.

Keywords AD · α7nAChR receptor · $A\beta_x$ fragments · Binding sites · Key residues

Introduction

Alzheimer's disease (AD) is the most common cause of dementia and characterized by cognitive decline and memory loss[1]. As the global population ages, the number of people with AD is increasing rapidly, posing significant health and economic challenges[2, 3]. The main pathological features of AD include the accumulation of beta-amyloid (Aβ) plaques in the brain and tau tangles as well as neuronal loss[2, 4]. Different Aβ species in length, including the two most abundant forms $A\beta_{1-40}$ and $A\beta_{1-42}$[5], are hydrolyzed from amyloid precursor protein (APP) and their aggregation drives disease progression. Self-assembly of $A\beta_{42}$ peptide chains and other hydrolytic product mutants leads to the accumulation of misfolded fibers, which are highly cytotoxic and thus contribute to neuronal death[6]. In addition, $A\beta_{42}$ has also been shown to be physiologically toxic at high concentrations, as it can alter neuronal signaling by interacting with α7 nicotinic acetylcholine receptor (α7nAChR), leading to synaptic dysfunction in AD patients[7].

Receptor binding experiments have shown that $A\beta_{1-42}$ has a high affinity for α7nAChR[8] and therefore inhibit the calcium activation and acetylcholine release, two processes closely associated with memory and cognitive function, but may be treated by disruption to the α7nAChR-$A\beta_{42}$ interaction[9]. For example, Richter MC's study (2018) indicated that direct application of the last 16 amino acids (CT16) at the C-terminus of sAPPα (lacking in sAPPβ) in the mouse hippocampus is beneficial to improve LTP effect and memory level and rescue hippocampal spine density in vitro by relying on functional nicotinic α7nAChR, thus confirming that the CT16 (it also is the first 16 amino acids $A\beta_{1-16}$ at the N-terminus of $A\beta_{42}$) acts as a potent enhancer of cholinergic signaling via α7nAChRs [10].

It still remains controversial for the neuroprotective role of a specific $A\beta_{42}$ fragment on the receptor. Under experimental physiological conditions, $A\beta_{42}$ can enhance

✉ Hongqi Ai
chm_aihq@ujn.edu.cn

[1] School of Chemistry and Chemical Engineering, University of Jinan, Jinan 250022, People's Republic of China

neuroplasticity and memory formation by increasing the release of presynaptic neurotransmitters[11, 12], while $A\beta_{12-28}$ peptide fragment was found to play a vital role for the function of $A\beta_{1-42}$. However, the immunoprecipitation experiment conducted by Wang et al.[13] also revealed that binding epitope for α7nAChR resides in the amino acid 12–28 sequence region ($A\beta_{12-28}$), rather than other Aβ peptide fragments, $A\beta_{1-11}$, $A\beta_{10-20}$, and $A\beta_{22-35}$ of $A\beta_{42}$, conflicting with the N-terminal epitope (e.g., $A\beta_{1-16}$) of $A\beta_{42}$ for α7nAChR binding. Their results also contradict with L. Michel whose paper delineating the binding site of the Aβ peptide[14]. From the simulation aspect, the $A\beta_{12-28}$ fragment completely tends to prevent the formation of α7nAChR-$A\beta_{42}$ complex, supporting that the key residues to the loop C of α7nAChR are in the 12V-28K region of the $A\beta_{42}$ peptide [8].

In addition, it is also disagreement over the identification for the key residues of these different Aβ fragments. Wang et al. identified that Y10 and H13 act as key residues of $A\beta_{42}$ for α7nAChR binding, inhibiting acetylcholine release and external expression of calcium flux, rather than internalizing neuroprotective effects[13] when $A\beta_{42}$ interacts to the receptor. By further shrinking the core sequence of N-terminal $A\beta_{1-16}$ fragment activity, an essential and unique core hexapeptide sequence $Y_{10}EVHHQ_{15}$ (Aβcore) was identified as effective as the $A\beta_{1-16}$ fragment in inducing Ca^{2+} responses[15]. Moreover, Aβcore and $A\beta_{1-16}$ show the similar neural regulatory effects with $A\beta_{42}$[16], where positive roles at positions H13 and H14 in initiating activity and reverse inhibition at Q15 were suggested[16]. In addition, the shorter hexapeptide core sequence protected or reversed Aβ-induced neuronal toxicity[17].

Aiming to these controversies and disagreements, four small peptide fragments of $A\beta_{1-16}$, $A\beta_{10-16}$, $A\beta_{12-28}$, and $A\beta_{30-42}$ were selected as ligands to explore both the mechanism of binding with receptor α7nAChR and details of the binding sites, so that the potential regulatory targets of α7nAChR at the molecular level[18] can be revealed.

Computational methods

Model design

The receptor α7nAChR (PDB ID: 7KOX) [19]used in this study was obtained from the RCSB database (https://www.rcsb.org/), from which only the ligand binding domain (LBD) are truncated (Fig. 1a-c) to build the receptor-ligand complex, as the LBD was taken as the main body of ligand binding [20, 21]. An α7nAChR contains five homomeric subunit structure, therefore displaying five identical LBDs for ligand binding. The fragment structure of ligand $A\beta_x$ were clipped from $A\beta_{42}$ (PDB ID of 1IYT[8]) individually subject to four peptide lengths using Pymol[22], $A\beta_{1-16}$ DAEFRHDSGYEVHHQK, $A\beta_{10-16}$ YEVHHQK, $A\beta_{12-28}$ VHHQKLVFFAEDVGSNK, and $A\beta_{30-42}$ AIIGLMVGGVVIA. Then LBD and $A\beta_x$ were docked together using the CABS-DOCK online protein–ligand docking server to obtained the top α7nAChR-$A\beta_x$ (α7-$A\beta_x$) complexes (http://biocomp.chem.uw.edu.pl/CABSdock/) [23, 24]. For each docking results, 10 complexes with the highest

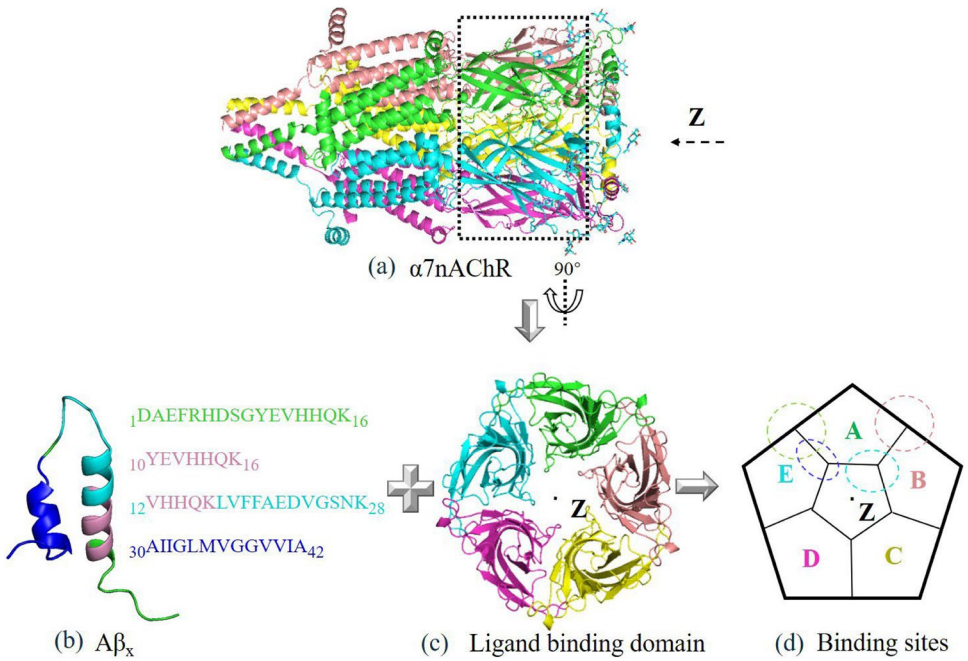

Fig. 1 Definition for the binding sites of α7nAChR. (**a**) Protein structure of α7nAChR. (**b**) The fragment conformations of $A\beta_x$, $A\beta_{1-16}$ in green, $A\beta_{10-16}$ in pink, $A\beta_{12-28}$ in light blue, $A\beta_{30-42}$ in dark blue, and the overlap between $A\beta_{10-16}$ and $A\beta_{12-28}$ is shown in pink. (**c**) Front view of ligand binding domain of α7nAChR, where five chains (subunits), A B, C, D, and E, are depicted in clockwise order as green, blue, pink, yellow, and orange, respectively. (**d**) The potential binding sites (highlighted in circle) accommodated by α7nAChR for any of the four peptide fragments

scores were selected, and the relevant data are shown in the Tables S1–S4 in Supporting Information (SI). Among them, only the first three α7-Aβ_x complex models with four available items scores (cluster density, average RMSD, max RMSD, number of elements) were subjected to the following molecular dynamics simulations. The docked conformations in Figure S1 show that Aβ_x prefers to lie at the interface between two adjacent α7 subunits, as indicated previously [25].

MD simulation details

These selected complex models were constructed using Charmm-GUI website[26]. Under periodic boundary conditions, Charmm36 force field[27] and TIP3P water model[28] were used to solve all systems. Additional Na^+ is used to neutralize the system [29]. The LINCS algorithm[30] was used to constrain the hydrogen bond length. For the bond length of water molecules, SETTLE constraint algorithm [31] is adopted, allowing the integration time step to be 2 fs. Before the MD simulation, the NVT ensemble balance for 100 ps was performed at a constant temperature (T = 310 K) using V-rescale temperature coupling[32], and the time constant was set as 0.1 ps. The NPT ensemble balance for 100 ps was carried out with a time constant of 2.0 ps at 310 K. All the simulations above were performed using the GROMACS v5.15 package [33, 34].

Analysis methods

We evaluate the quality of MD models using root mean square deviation (RMSD) and root mean square fluctuation (RMSF) by choosing Cα. MMPBSA (Molecular Mechanics Poisson-Boltzmann Surface Area) is employed to perform binding free energy ($\Delta G_{binding}$) calculation. Molecular Mechanics/Poisson-Boltzmann Surface Area (MM/PBSA) is a widely utilized approach for post-processing molecular dynamics (MD) trajectories to estimate binding free energies[35–37]. It has been extensively applied in the field of molecular recognition[38]. In this study, we apply the MM/PBSA method to calculate the binding affinity between α7nAChR and Aβ_x, as well as to assess the contribution of each residue involved in the binding process, which helps to identify key interacting residues.

However, the conventional MM/PBSA method may overestimate the shielding effect when studying binding capabilities, leading to theoretical values that often significantly deviate from experimental data. To address this issue, Huang et al.[39] introduced a novel correction method that involves multiple linear regressions for various systems. This method provides a correction for the electrostatic and polar solvation terms, resulting in a highly adaptable fitting formula that is widely applicable, as shown in Eq. (6) in SI. So calculated $\Delta G_{binding/fitted}$ were used to convert into dissociation constant K_d for a conveniently comparison to the experimental values via following formulas (1) and (2).

$$K_d = e^{\frac{\Delta G_{binding/fitted}}{RT}} \quad (1)$$

$$\Delta G_{binding/fitted} = RT \cdot \ln K_d \quad (2)$$

where R is a constant with the value of 8.314 J/mol·K and T is 310 K. VMD[40] and PYMOL[41] are employed for conformational visualization.

Results and discussion

Conformational fluctuation of α7nAChR induced by Aβ_x binding

The RMSD value of α7nAChR in the α7-Aβ_x was calculated based on their backbone carbon atoms and shown in Figure S2 in SI, confirming that all of these complexes have reached equilibrium. The trajectories in the equilibrium stage are intercepted for RMSF fluctuation analysis.

Binding sites of α7nAChR for Aβ_x binding and the corresponding RMSFs

A$\beta_{1–16}$ is perpendicular to the Z axis and locating between chain A and chain B, biased to the bottom of the gap between the two chains, and mostly toward the loop C of chain A (Figure 2a). Residues in α7nAChR of α7-A$\beta_{1–16}$ with RMSF over 0.7 nm are S50, W114, S611 and S798, rewritten as S50 (A), W114(A), S611(D), and S798(E), due to their derived from chains A, D, and E, respectively. Analogously hereinafter the same below. Therefore, the great fluctuation of S50(A) and W114(A) are directly affected by A$\beta_{1–16}$ binding, but that of S611(D) and S798(E) are indirectly.

A$\beta_{10–16}$ lies at the top of the gap between chain A and chain B and also perpendicular to the Z axis. The overall structure of A$\beta_{10–16}$ is in the top Cys-loop[16] of the chain B, resulting in larger fluctuation (> 0.6 nm) of residues E153(B), F302(B), C357(B), S423(C), R748(D), and E799(E) in α7nAChR. Obviously, the first three residues of E153(B), F302(B), C357(B) have a direct effect upon A$\beta_{10–16}$ binding.

A$\beta_{12–28}$ is located perpendicular to the Z axis at the top of the gap between chain A and chain E, and most of the structure is near the Cys-loop region of chain E. P188(B), F491(C), P562(D), and R914(E) show significant fluctuations compared with other residues in α7-A$\beta_{12–28}$. The location is mutually verified with the position results presented by the experiment[13]. Highly conserved residues in loop C

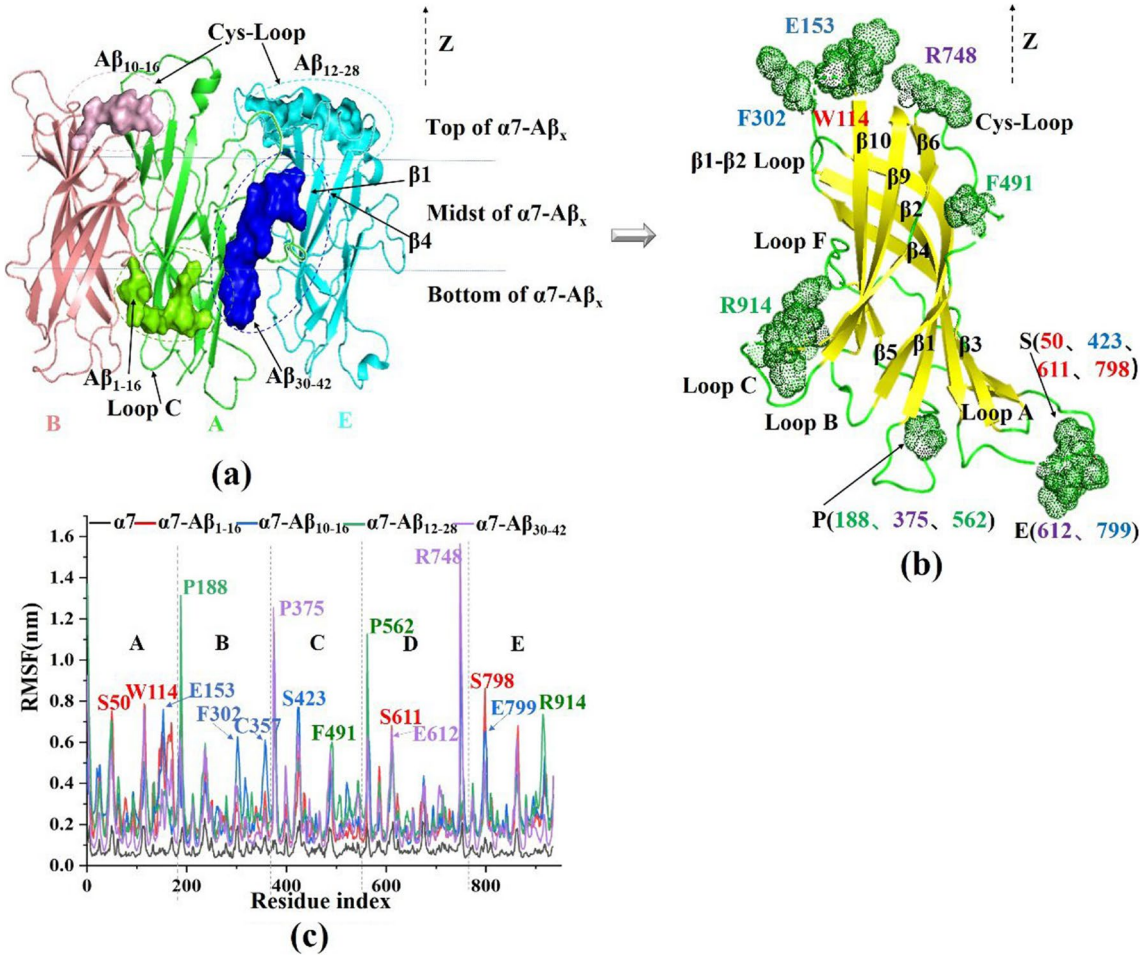

Fig. 2 (**a**) 3D definition for the binding sites of α7nAChR in α7-Aβ_{1-16} (in green), α7-Aβ_{10-16} (in pink), α7-Aβ_{12-28} (in light blue), and α7-Aβ_{30-42} (in blue), respectively. These Aβx fragments are mainly locating among subunits A, B, and E of α7nAChR. One of five symmetric subunits of α7nAChR is displayed in (**b**) so that the identical and symmetric residues in these subunits can be converged on and compared. In addition, the color of the residue serial number in (**b**) corresponds to the RMSF color of the complex in (**c**). For example, RMSF result of α7-Aβ_{1-16} is displayed in red, and high fluctuation of S50 in the complex is observed, and therefore the corresponding number of 50 in (**b**) is shown in red. (**c**) RMSF (nm) of α7nAChR in α7nAChR alone (in black) and in complexes of α7-Aβ_{1-16} (in red), α7-Aβ_{10-16} (in blue), α7-Aβ_{12-28} (in green), and α7-Aβ_{30-42} (in purple), respectively

is not only a binding site, but also a determinant in the activatory or inhibitory effect of the Aβ on the a7nAChR [42].

Most of the Aβ_{30-42} structure is parallel to the β1 and β4 regions of chain A and chain E, speculating that it is because 10 hydrophobic residues (A30-I32, L34-V36, V39-A42) in Aβ_{30-42} keep it away from the flexible loop region at both ends of the receptor chain E. Aβ_{30-42} impacts strongly to W114(A), P375(C), P490(C), P562(D), E612(D), and R748(D), suggesting that Aβ_{30-42} make these residues more unstable and have greater potential to interact with the receptor. Among them, only W114 has direct effect as it is just at the junction of the chains A and E, while P375(C), P490(C), P562(D), E612(D), and R748(D) influence Aβ_{30-42} through other indirect ways of action.

To normalize the relative location of the same residue in different chains of the α7nAChR, the first subunit of α7nAChR (chain A with residues of 1–187) is displayed in Figure 2b, where the different loop regions are defined, as did in ref[43], and the key fluctuation residues are displayed in dotted surface and colored in label corresponding to that of Aβ_x fragment in Figure 2c.

First, the identical residue of serine in three different chains of receptor α7nAChR is observed to interact with Aβ_{1-16} fragment in great fluctuation, indicating that the fragment is locating at loop A and perpendicular to *Z* axis.

For α7-Aβ_{10-16}, two residues, E153(B) and F302(B) of α7nAChR with higher RMSF, are highlighted in Fig. 2b, induced by the direct interaction of the Aβ_{10-16} at the Cys-loop. Interestingly, there are also two residues S423(C) and E799(E) greatly fluctuated, which are at the loop A, the opposite loop of location of Aβ_{10-16}, presenting stronger effector-receptor effect. The strongest fluctuation induced

by $A\beta_{12-28}$ are from residues P188(B) and P562(D), which are displayed on the chains B and D, contributing to the loop B, very close to loop A, where $A\beta_{1-16}$ is just locating. The residues P375(C) and R748(D) have the largest fluctuation in α7-$A\beta_{30-42}$, but locate at the two loops, both ends of α7nAChR, indicating the indirect effect of $A\beta_{30-42}$ binding as the fragment of $A\beta_{30-42}$ is locating at the middle of the chain (Fig. 2a).

RMSFs of $A\beta_x$

It can be intuitively seen from Fig. 3 that $A\beta_{1-16}$ is overwhelmingly more flexible than other $A\beta_x$ species, and the RMSFs with the most remarkable fluctuation (> 1.5 nm) are mainly contributed by the Y10-K16 residues of $A\beta_{1-16}$. It is almost twice as high as the corresponding counterparts of residues in both $A\beta_{10-16}$ (Aβcore) and $A\beta_{12-28}$. Notably, the largest fluctuation regions in $A\beta_{1-16}$, $A\beta_{12-28}$, and $A\beta_{10-16}$ are residues 10–16, echoing the common observation of neuroprotective role to α7nAChR for the three fragments [10, 13, 15] although they are so different as mentioned above. By contrast, the RMSF values of $A\beta_{30-42}$ is so low due to its more hydrophobic residues and weaker interaction with the α7nAChR receptor.

In the α7-$A\beta_x$ complex, E11 and V12 in $A\beta_{1-16}$ fragment are contacting with two positively charged residues, K182 and R183 of the receptor within a distance of 5 Å. Based on the observed RMSF fluctuation patterns, it can be inferred that the primary interaction region between any of the three $A\beta_x$ fragments, $A\beta_{1-16}$, $A\beta_{10-16}$, and $A\beta_{12-28}$, and α7nAChR may be confined to the Y10-K16 segment. This inference aligns with existing experimental literature, which has identified Y10-K16 as a critical binding region for $A\beta_x$ with α7nAChR[44]. Furthermore, Daniel H. S. Lee and colleagues have demonstrated through co-immunoprecipitation experiments that residues Y10 and H13 within the loop can indeed form complexes with α7nAChR[13]. These findings collectively support the notion that the Y10-K16 region is a key binding domain for the interaction between $A\beta_x$ and α7nAChR, highlighting the importance of this region in the molecular recognition and subsequent biological effects of $A\beta_x$ on the receptor.

Binding residues and contact area on the interface

When $A\beta_{1-16}$ contacts with α7nAChR, the contributing residues on interface are of Y129(A), Q140(A), G181(A), K182(A), R183(A), S184(A), and I169(B) and L38(B) from α7nAChR and A2, E3, R5, H6, S8, G9, Y10, V12, and K16 in $A\beta_{1-16}$ (Fig. 4b), where R5 contributes the most the contact area of 203.2 $Å^2$ and accounts for 25.1% of total residue contributions, being confirmed as the main active residue by immune coprecipitation[13]. Apparently, the ARG residue play the dominant role for the receptor-peptide contact in α7-$A\beta_{1-16}$ complex.

In α7-$A\beta_{10-16}$, the key contact residues at the interface are T30(A), Y32(A), E162(A), D164(A), S113(A) of α7nAChR and K7, Y10, and H5 of $A\beta_{10-16}$, respectively. The total contact areas of K7, Y10, and H5 were all above 120.0 $Å^2$, while Y10 was 141.4 $Å^2$, consistent with the experimental observation on the activity assay that the mutation at residue Y10 instead of E11 and V12 plays a key role in the active center through partial aromatic groups and hydroxyl groups in Aβ core[45]. Moreover, Y10 is identified as the key contact residue in both α7-$A\beta_{1-16}$ and α7-$A\beta_{10-16}$.[13] The contribution value of Y10 is more prominent in $A\beta_{10-16}$ (17.37%) than in $A\beta_{1-16}$(8.61%). By contrast, the key R5 contribution observed in α7-$A\beta_{1-16}$ is absent in α7-$A\beta_{10-16}$ due to the truncation of the first nine residues in $A\beta_{10-16}$, indicating a potential effect on the active function.

In α7-$A\beta_{12-28}$, the main contact residues are C190(E), K192(E), and W154(E) of α7nAChR and F19, K16, and V12 of $A\beta_{12-28}$, in which larger contact areas of 250.5$Å^2$ and 213.1$Å^2$ for K16 and F19, respectively, are observed.

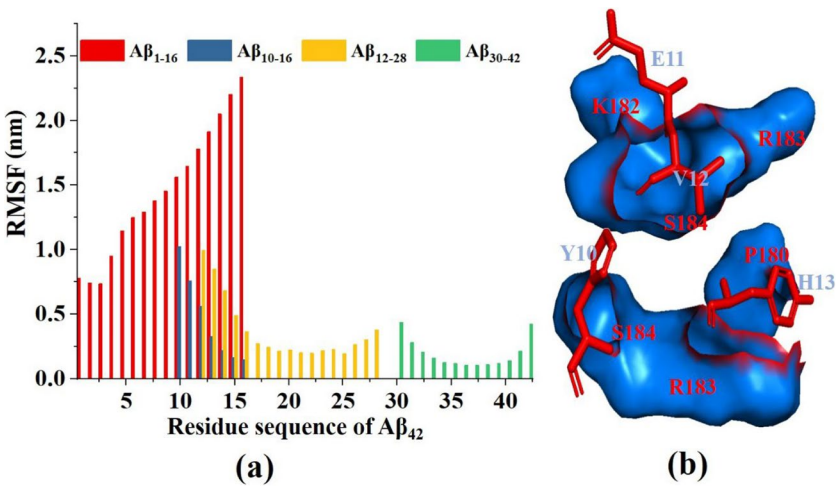

Fig. 3 (**a**) RMSFs (nm) of $A\beta_{1-16}$, $A\beta_{10-16}$, $A\beta_{12-28}$, $A\beta_{30-42}$ in their α7-$A\beta_x$ complexes, respectively, and (**b**) relative positions of four key residues E11, V12, Y10, H13 in the complexes

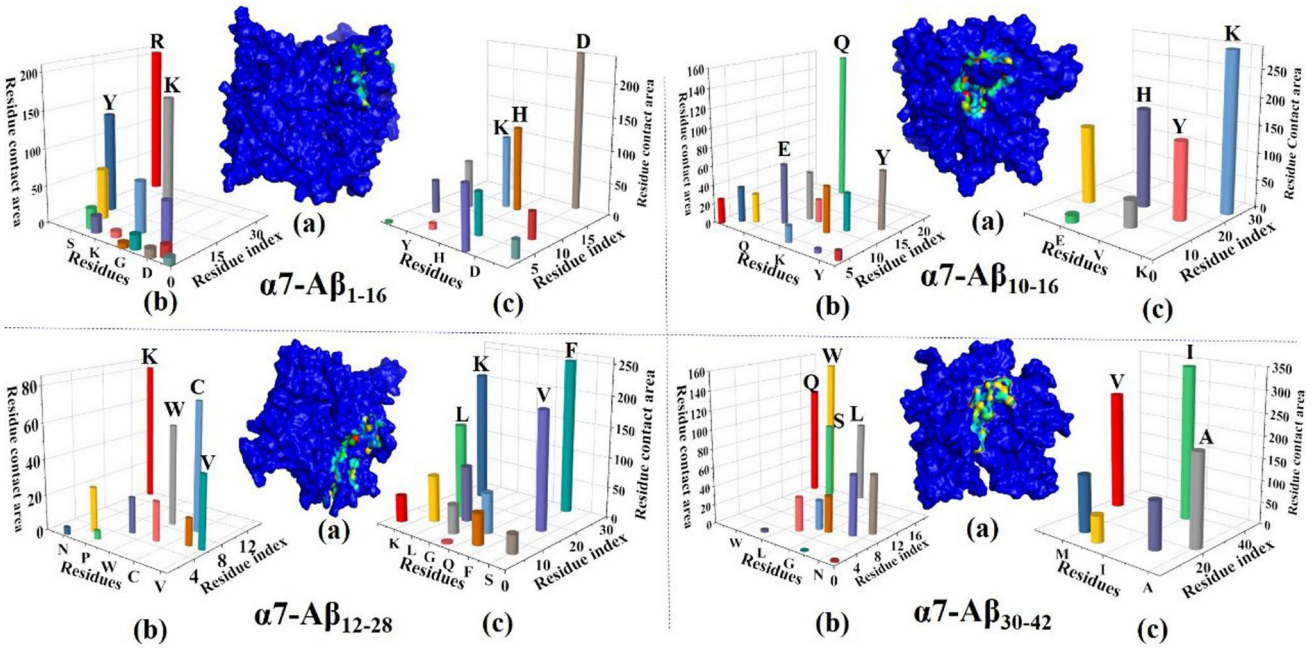

Fig. 4 Contact area (Å^2) of major residues at interface between any of four fragments $A\beta_{1–16}$, $A\beta_{10–16}$, $A\beta_{12–28}$, $A\beta_{30–42}$, and α7nAChR, respectively. (**a**) Binding residues at the interface are shown in light color, relative to the surrounding residues in dark blue. (**b**) and (**c**) display the contact areas of residues from α7nAChR and $A\beta_x$, respectively, in α7-$A\beta_{1–16}$, α7-$A\beta_{10–16}$, α7-$A\beta_{12–28}$, and α7-$A\beta_{30–42}$ complexes

Among the three key contact residues, V12 is a reserved one, same as that in $A\beta_{1–16}$ and $A\beta_{10–16}$.

Anyway, four residues, Y10, V12, H13, and K16, locate at the contact interface in the three α7-$A\beta_x$ complexes, which is consistent with the results of biological experiment[13, 15, 17], although there are large differences in the contribution ratio for the four residues in α7-$A\beta_{1–16}$ (8.61%, 5.97%, 15.27%, 13.06%), α7-$A\beta_{10–16}$ (17.37%, 6.05%, 21.98%, 35.58%), and α7-$A\beta_{12–28}$(0, 15.89%, 0.22%, 17.58%), respectively.

When it comes to α7-$A\beta_{30–42}$, the main residues at the contact interface are Q117(E), W55(E), S59(E), and L38(A) in β1 and β4 of α7nAChR and A30, I32, and V36 of $A\beta_{30–42}$. All of them are hydrophobic, accounting for why $A\beta_{30–42}$ fragment prefers to locate over the β1 and β4-sheets rather than the loop regions.

Binding energy and residue contributions

The binding free energy (ΔG_{bind}) is decomposed into five terms: van der Waals force (ΔE_{VDW}), electrostatic interaction force (ΔE_{COU}), polar solvation energy (ΔG_{PB}), non-polar solvation energy (ΔG_{SA}), and entropic contribution ($-T\Delta S$).

As shown in Table 1, different dominant forces contributing to the overall binding energy are observed for these different α7-$A\beta_x$ complexes. For example, in the α7-$A\beta_{1–16}$ complex, ΔE_{VDW} (van der Waals force) is dominant in the contribution of binding free energy, and the absolute value of −29.6 kJ/mol is much higher than the ΔG_{SA} (non-polar solvation energy, −8.9 kJ/mol) and plays a major role in promoting the specific binding of the complex, so does for the binding between $A\beta_{10–16}$ and α7nAChR, where the ΔE_{VDW} is also more prominent at −118.6 kJ/mol. For the α7-$A\beta_{12–28}$ complex, electrostatic interaction force (ΔE_{COU}) rather than the ΔE_{VDW} is the main driving force, indicating that the Coulomb interaction plays the dominant role in binding between α7nAChR

Table 1 Binding energies (kJ/mol) of top complex between α7nAChR and $A\beta_x$

Complexes	ΔE_{VDW}	ΔE_{COU}	ΔG_{PB}	ΔG_{SA}	$-T\Delta S$	ΔG_{bind}	$\Delta G_{bind/fitted}$
α7-$A\beta_{1–16}$	−29.6	−23.8	15.1	−8.9	16.3	−7.3	−8.3
α7-$A\beta_{10–16}$	−118.6	−96.7	196.2	21.7	21.1	−4.7	−13.4
α7-$A\beta_{12–28}$	−160.7	−368.7	495.2	−29.5	38.2	−6.1	−19.1
α7- $A\beta_{30–42}$	−16.5	−18.6	3.5	−6.8	3.3	−8.4	−8.9

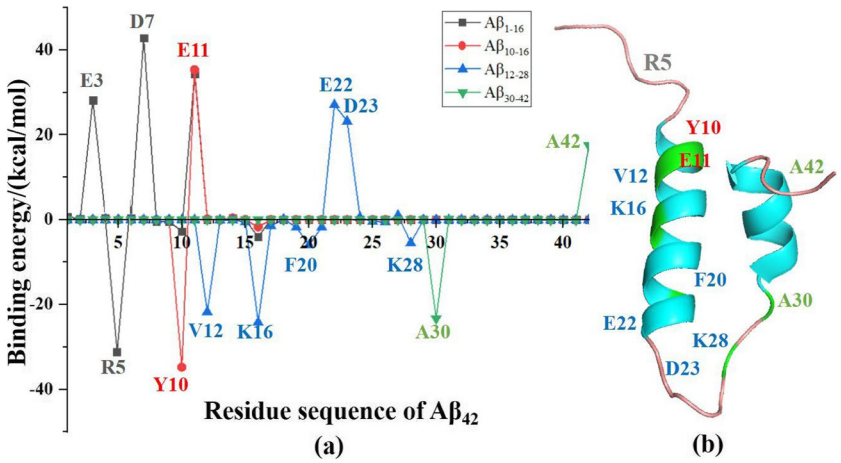

Fig. 5 (**a**) The residue contribution of $A\beta_{1–16}$, $A\beta_{10–16}$, $A\beta_{12–28}$, and $A\beta_{30–42}$ fragments to the binding free energy in the α7-$A\beta_x$ complexes. (**b**) Location of the major binding residues in $A\beta_{42}$

and $A\beta_{12–28}$, so does for the α7-$A\beta_{30–42}$ complex, indicating that both α7-$A\beta_{30–42}$ and α7-$A\beta_{12–28}$ can be classified as a group of "Coulomb interaction," whereas both α7-$A\beta_{1–16}$ and α7-$A\beta_{10–16}$ as the group of "van der Waals interaction."

The dissociation constant $K_d = 9.0$ μM was measured in the experiment[7] using α7nAChR and $A\beta_{1–42}$ as the receptor and ligand, respectively. The value can be converted into − 12.1 kJ/mol, being less than that (− 13.4 vs − 19.1 kJ/mol) of α7-$\beta_{10–16}$ and α7-$A\beta_{12–28}$, larger than that (−8.3 kJ/mol) of α7-$A\beta_{1–16}$ predicted in the present paper. The differences are ascribed to the $A\beta_x$ distinction. In other words, these values are reasonably consistent with each other if either different length or residue types of these $A\beta_x$ fragments are not taken into account. When it comes to the calculation and conversion process, please see the relevant details in the supporting materials.

To simplify the analysis, the residue contributions from four peptide fragments $A\beta_x$ are presented in Fig. 5, where Y10 shows outstanding binding energy contributions that are −2.76 and −34.75 kcal/mol, respectively, in $A\beta_{1–16}$ and $A\beta_{10–16}$. Although the energy of Y10 in α7-$A\beta_{1–16}$ is far weaker than that in α7-$A\beta_{10–16}$, it is stronger than that (−0.08 kcal/mol) of Q15 however, becoming the second top contribution to the binding energy of α7-$A\beta_{1–16}$. The determinant or top contribution comes from R5 (−33.99 kcal/mol), which is absent in the α7-$A\beta_{10–16}$. Therefore, the three residues contribute to the stability of the α7-$A\beta_{1–16}$ complex. On the other hand, three negatively charged D7, E3, and E11 residues disfavor to the instability of the complex, as their binding energies are positive values.

In contrast, Y10 binding energy of $A\beta_{10–16}$ in α7-$A\beta_{10–16}$ was significantly enhanced (−34.75 kcal/mol), but almost offset by its nearby E11 (35.37 kcal/mol). Therefore, the contribution from K16 becomes indispensable and even very important, although it is minor. In the α7-$A\beta_{12–28}$ complex, the binding energy contribution K28 on $A\beta_{12–28}$ is −5.44 kcal/mol, an important value to the stability of the α7-$A\beta_{12–28}$ complex, consistent with the experimental findings that residue V28 is the key recognition site to the α7nAChR[13]. Obviously, there is no such residue in both $A\beta_{1–16}$ and $A\beta_{10–16}$ fragments. Moreover, the major contribution residues in $A\beta_{12–28}$ are different from those of either $A\beta_{1–16}$ or $A\beta_{10–16}$, and the two key residues V12 and K16 in the common Aβcore region become the major binding contributors to the stability of $A\beta_{12–28}$. By contrast, only K16 is the unique one to contribute to the stability of α7-$A\beta_x$ complex, no matter the $A\beta_x$ fragment is $A\beta_{1–16}$, $A\beta_{10–16}$ or $A\beta_{12–28}$. Residue contributions of $A\beta_{30–42}$ in α7-$A\beta_{30–42}$ are unique exception, in which the key contributions of two hydrophobic residues A30 and A42 are observed, and absent in any of other three $A\beta_x$ fragments, verifying that only $A\beta_{1–16}$, $A\beta_{10–16}$, or $A\beta_{12–28}$ other than $A\beta_{30–42}$ was observed to be neuroprotective[13].

Conclusions

Even all of these $A\beta_x$ fragments $A\beta_{1–16}$, $A\beta_{10–16}$, and $A\beta_{12–28}$ rather than $A\beta_{30–42}$ are identified as neuroprotective ligands by binding to α7nAChR, the specific and distinctive roles they played at the molecular level remain to be probed, and therefore, it becomes the contribution of the study.

$A\beta_{1–16}$ prefers to locate at the Loop C region with a perpendicular pose at the bottom of the chain A and B in α7-$A\beta_{1–16}$. The contact area and residue number of $A\beta_{1–16}$ are more than that of $A\beta_{10–16}$, which provides speculation and explanation for the differences in the two different reactions. The contact residues of $A\beta_{1–16}$ involve Y10, E11, V12, and H13 of $A\beta_{1–16}$ and of α7nAChR contain P180, K182, R183, and S184.

$A\beta_{10–16}$ prefers to locate at the Cys-loop region with a perpendicular pose to the *Z* axis in the top of the chains A and B in α7-$A\beta_{10–16}$. Y10 and H13 in $A\beta_{10–16}$ are not as prominent as them in $A\beta_{1–16}$, which could be explained by

the particular D1-G9 section in $A\beta_{1-16}$. In the Cys-loop top region of α7-$A\beta_{10-16}$ complex, the L156-G167 sequence is within 2 Å distance from Y10 and K16, which is the main interaction region.

$A\beta_{12-28}$ in α7-$A\beta_{12-28}$ prefers to locate the bottom Cys-loop region of the complex and is perpendicular to the *Z* axis. The P21-Q27 and S26-F33 sequences are within 3 Å distance from L17 and K28 of $A\beta_{12-28}$, indicating the main interaction region. K28 in $A\beta_{12-28}$ plays the major role in the interaction with the receptor protein.

$A\beta_{30-42}$ in α7-$A\beta_{30-42}$ is an exception, an artificial ligand to probe why such a fragment cannot play the similar protective role to the first three fragments. That is, the parallel location to the *Z* axis, rich-hydrophobic interaction and consequently far from the loop regions account for all of these questions.

The limitation of the study is lack of the discussion on structure–function relationship, resulting in the failing in intuitive impression on the specific function of these different $A\beta_x$ fragments upon binding α7nAChR. At least, we displayed the radius changes of ion channel of α7nAChR induced by the binding of different $A\beta_x$ fragments (Figure S3), which is worthy of further exploration.

Supplementary Information The online version contains supplementary material available at https://doi.org/10.1007/s00894-024-06032-w.

Author contribution X. G. was responsible for the implementation, writing, and revision of this manuscript. Y. G. contributed to validation. C. W. and M. J. provided data analysis and methodology discussion. S. A. and M. F. N. assist the expression of the article. H. A. raised the idea and performed the final revisions. All authors reviewed the final version of the manuscript.

Funding This work was supported by the Shandong Provincial Natural Science Foundation (ZR2022MB073) of China.

Data availability No datasets were generated or analyzed during the current study.

Declarations

Competing interests The authors declare no competing interests.

References

1. Selkoe DJ (2001) Physiol Rev 81:741
2. Gulyaeva NV (2021) J Neurochem 156:399
3. Sagar SR, Singh DP, Panchal NB, Das RD, Pandya DH, Sudarsanam V, Nivsarkar M, Vasu KK (2018) ACS Chem Neurosci 9:1663
4. Baptista FI, Henriques AG, Silva AMS, Wiltfang J (2014) da Cruz e Silva, O. A. B. ACS Chem Neurosci 5:83
5. Selkoe D (2002) J Sci 298:789
6. Michaels TCT, Šarić A, Curk S, Bernfur K, Arosio P, Meisl G, Dear AJ, Cohen SIA, Dobson CM, Vendruscolo M, Linse S, Knowles TPJ (2020) Nat Chem 12:445
7. Cecon E, Dam J, Luka M, Gautier C, Chollet AM, Delagrange P, Danober L, Jockers R (2019) Br J Pharmacol 176:3475
8. Espinoza-Fonseca LM (2004) Biochem Biophys Res Commun 320:587
9. Wang HY, Trocme-Thibierge C, Stucky A, Shah SM, Kvasic J, Khan A, Morain P, Guignot I, Bouguen E, Deschet K, Pueyo M, Mocaer E, Ousset PJ, Vellas B, Kiyasova V (2017) Alzheimers Res Ther 9:54
10. Richter MC, Ludewig S, Winschel A, Abel T, Bold C, Salzburger LR, Klein S, Han K, Weyer SW, Fritz AK, Laube B, Wolfer DP, Buchholz CJ, Korte M, Müller UC (2018) Embo J 37:11
11. Yang P, Perlmutter JS, Benzinger TLS, Morris JC, Xu J (2020) Ageing Res Rev 57:100994
12. Müller UC, Deller T, Korte M (2017) Nat Rev Neurosci 18:281
13. Wang H-Y, Lee DHS, D'Andrea MR, Peterson PA, Shank RP, Reitz AB (2000) J Biol Chem 275:5626
14. Espinoza-Fonseca LM (2004) Biochem Biophys Res Commun 323:1191
15. Lawrence JLM, Tong M, Alfulaij N, Sherrin T, Contarino M, White MM, Bellinger FP, Todorovic C, Nichols RA (2014) J Neurosci 34:14210
16. Forest KH, Alfulaij N, Arora K, Taketa R, Sherrin T, Todorovic C, Lawrence JLM, Yoshikawa GT, Ng HL, Hruby VJ, Nichols RA (2018) J Neurochem 144:201
17. Dinamarca MC, Raveh A, Schneider A, Fritzius T, Früh S, Rem PD, Stawarski M, Lalanne T, Turecek R, Choo M, Besseyrias V, Bildl W, Bentrop D, Staufenbiel M, Gassmann M, Fakler B, Schwenk J, Bettler B (2019) Nat Commun 10:1331
18. Skeby KK, Sorensen J, Schiott B (2013) J Am Chem Soc 135:15114
19. Noviello CM, Gharpure A, Mukhtasimova N, Cabuco R, Baxter L, Borek D, Sine SM, Hibbs RE (2021) Cell 184:2121
20. Bertrand D, Lee CH, Flood D, Marger F, Donnelly-Roberts D (2015) Pharmacol Rev 67:1025
21. Arias HR (2000) Neurochem Int 36:595
22. Mooers BHM (2020) Protein Sci 29:268
23. Blaszczyk M, Ciemny MP, Kolinski A, Kurcinski M, Kmiecik S (2019) Briefings Bioinf 20:2299
24. Blaszczyk M, Kurcinski M, Kouza M, Wieteska L, Debinski A, Kolinski A, Kmiecik S (2016) Methods 93:72
25. Xu L, Zhang X, Feng Q, Zheng Y, Ni H, Shen H, Yao M (2019) ACS Chem Neurosci 10:497
26. Jo S, Kim T, Iyer VG, Im W (1859) J Comput Chem 2008:29
27. Lee J, Cheng X, Swails JM, Yeom MS, Eastman PK, Lemkul JA, Wei S, Buckner J, Jeong JC, Qi Y, Jo S, Pande VS, Case DA, Brooks CL 3rd, MacKerell AD Jr, Klauda JB, Im W (2016) J Chem Theory Comput 12:405
28. Jorgensen WL, Chandrasekhar J, Madura JD, Impey RW, Klein ML (1983) J Chem Phys 79:926
29. Mudedla SK, Murugan NA, Agren H (2019) ACS Chem Neurosci 10:1347
30. Hess B, Bekker H, Berendsen HJC, Fraaije JGEM (1997) J Comput Chem 18:1463
31. Qiu Y, Mekkat A, Yu H, Yigit S, Hamaia S, Farndale RW, Kaplan DL, Lin YS, Brodsky B (2018) J Comput Chem 203:255
32. Eslami H, Mojahedi F, Moghadasi J (2010) J Chem Phys 133:084105
33. Pronk S, Páll S, Schulz R, Larsson P, Bjelkmar P, Apostolov R, Shirts MR, Smith JC, Kasson PM, van der Spoel D, Hess B, Lindahl E (2013) Bioinformatics 29:845
34. Hess B, Kutzner C, van der Spoel D, Lindahl E (2008) J Chem Theory Comput 4:435
35. Rahman MU, Liu H, Wadood A, Chen HF (2016) Mol Biosyst 12:3280
36. Yu H, Fang Y, Lu X, Liu Y, Zhang H (2014) Chem Biol Drug Des 83:89

37. Martin TD, Hill EH, Whitten DG, Chi EY, Evans DG (2016) Langmuir 32:12542
38. Miller BR, McGee TD, Swails JM, Homeyer N, Gohlke H, Roitberg AE (2012) J Chem Theory Comput 8:3314
39. Huang K, Luo S, Cong Y, Zhong S, Zhang JZH, Duan L (2020) Nanoscale 12:10737
40. Humphrey W, Dalke A, Schulten K (1996) J Mol Graphics Modell 14:33
41. Rigsby RE, Parker AB (2016) Biochem Mol Biol Educ 44:433
42. Baumketner A, Shea J-E (2006) J Mol Biol 362:567
43 Zhao Y, Liu S, Zhou Y, Zhang M, Chen H, Eric XuH, Sun D, Liu L, Tian C (2021) Cell Res 31:713
44. Gong Y, Huang A, Guo X, Jia Z, Chen X, Zhu X, Xia Y, Liu J, Xu Y, Qin X (2021) Chem Eng J 418:129345
45. Tong M, Arora K, White MM, Nichols RA (2011) J Biol Chem 286:34373